BBA - Biomembranes 1864 (2022) 183836

Contents lists available at ScienceDirect

BBA - Biomembranes

journal homepage: www.elsevier.com/locate/bbamem

Probing the local secondary structure of bacteriophage S^{21} pinholin membrane protein using electron spin echo envelope modulation spectroscopy

Daniel L. Drew Jr [a], Tanbir Ahammad [a], Rachel A. Serafin [a], Indra D. Sahu [b,a], Rasal H. Khan [a], Emily Faul [a], Robert M. McCarrick [a], Gary A. Lorigan [a,*]

[a] Department of Chemistry and Biochemistry, Miami University, Oxford, OH 45056, USA
[b] Natural Science Division, Campbellsville University, Campbellsville, KY 42718, USA

ARTICLE INFO

Keywords:
Holin
Pinholin
EPR spectroscopy
ESEEM
Secondary structure

ABSTRACT

There have recently been advances in methods for detecting local secondary structures of membrane protein using electron paramagnetic resonance (EPR). A three pulsed electron spin echo envelope modulation (ESEEM) approach was used to determine the local helical secondary structure of the small hole forming membrane protein, S^{21} pinholin. This ESEEM approach uses a combination of site-directed spin labeling and ^{2}H-labeled side chains. Pinholin S^{21} is responsible for the permeabilization of the inner cytosolic membrane of double stranded DNA bacteriophage host cells. In this study, we report on the overall global helical structure using circular dichroism (CD) spectroscopy for the active form and the negative-dominant inactive mutant form of S^{21} pinholin. The local helical secondary structure was confirmed for both transmembrane domains (TMDs) for the active and inactive S^{21} pinholin using the ESEEM spectroscopic technique. Comparison of the ESEEM normalized frequency domain intensity for each transmembrane domain gives an insight into the α-helical folding nature of these domains as opposed to a π or 3_{10}-helix which have been observed in other channel forming proteins.

1. Introduction

Membrane proteins are responsible for a wide variety of cellular functions including transport, signaling, lysis, and are targets for over 50% of small molecule drug binding [1–3]. However, determining membrane protein secondary structure has proved to be a challenge for the scientific community due to their hydrophobic nature, poor overexpression yields, and lack of high quality crystals [4,5]. Previously, the Lorigan group has demonstrated the electron spin echo envelope modulation (ESEEM) spectroscopy coupled with site directed spin labeling (SDSL) and isotopic amino acid labeling can be utilized to determine the local secondary structure of model membrane proteins [6–9]. This ESEEM technique was previously used to differentiate between α-helices and β-sheets as well as detect the presence of α-helices versus 3_{10}-helices [6–8]. The use of this ESEEM technique is advantageous over other biophysical structural techniques, like circular dichroism (CD) spectroscopy, as it can selectively probe local secondary structure as opposed to global structure. Knowing the local secondary structure is critical as changes in local structure have been shown to affect the packing of membrane proteins as well as their incorporation and interactions with the surrounding lipid environment [10]. There are also families of membrane proteins, that take part in a variety of cellular processes, which must undergo local conformational changes and refolding of their secondary structure to perform their ultimate function [11,12]. This ESEEM approach therein overcomes limitations seen in CD or NMR and supplies a method for determining these subtle, yet crucial changes in the local structure of peptides and proteins.

This ESEEM secondary structure technique requires a deuterated amino acid side chain (e.g. d_{10}-Leu) with a site-specific nitroxide spin label placed within four amino acids of the deuterated amino acid. A nitroxide spin label, in this case *S*-(1-oxyl-2,2,5,5-tetramethyl-2,5-dihydro-1H-pyrrol-3-yl)methyl methanesulfonothioate (MTSL), was attached via disulfide bond formation to the substituted cysteine sidechain. ESEEM spectroscopy detects the weak dipole-dipole interactions between the unpaired electron of the spin label and the deuterium of the labeled Leu sidechain within a detection limit of 8 Å [13,14]. The characteristic periodicity of helices and the linear nature of β-sheets reveals unique patterns in the ESEEM spectra as the spin label is moved

* Corresponding author at: 651 E. High St., Oxford, OH 45056, USA.
E-mail address: lorigag@miamioh.edu (G.A. Lorigan).

https://doi.org/10.1016/j.bbamem.2021.183836
Received 24 June 2021; Received in revised form 23 November 2021; Accepted 29 November 2021
Available online 11 December 2021

Table 1
Active and inactive pinholin S^{21} primary sequence.

Active S^{21}68		
Leu25	i-2	MDKISTGIAYGTSAGSAGY***X***F***i***QWLDQVSPSQWAAIGVLGSLVLGFLTYLTNLYFKIREDRRKAARGE
	i-3	MDKISTGIAYGTSAGSAG***X***WF***i***QWLDQVSPSQWAAIGVLGSLVLGFLTYLTNLYFKIREDRRKAARGE
	i-4	MDKISTGIAYGTSAGSA***X***YWF***i***QWLDQVSPSQWAAIGVLGSLVLGFLTYLTNLYFKIREDRRKAARGE
Leu50	i-2	MDKISTGIAYGTSAGSAGYWFLQWLDQVSPSQWAAIGVLGSLVL***X***F***i***TYLTNLYFKIREDRRKAARGE
	i-3	MDKISTGIAYGTSAGSAGYWFLQWLDQVSPSQWAAIGVLGSLV***X***GF***i***TYLTNLYFKIREDRRKAARGE
	i-4	MDKISTGIAYGTSAGSAGYWFLQWLDQVSPSQWAAIGVLGSL***X***LGF***i***TYLTNLYFKIREDRRKAARGE

Inactive S^{21}IRS		
Leu25	i-2	MRYIRSDKISTGIAYGTSAGSAGY***X***F***i***QWLDQVSPSQWAAIGVLGSLVLGFLTYLTNLYFKIREDRRKAARGE
	i-3	MRYIRSDKISTGIAYGTSAGSAG***X***WF***i***QWLDQVSPSQWAAIGVLGSLVLGFLTYLTNLYFKIREDRRKAARGE
	i-4	MRYIRSDKISTGIAYGTSAGSA***X***YWF***i***QWLDQVSPSQWAAIGVLGSLVLGFLTYLTNLYFKIREDRRKAARGE
Leu50	i-2	MRYIRSDKISTGIAYGTSAGSAGYWFLQWLDQVSPSQWAAIGVLGSLVL***X***F***i***TYLTNLYFKIREDRRKAARGE
	i-3	MRYIRSDKISTGIAYGTSAGSAGYWFLQWLDQVSPSQWAAIGVLGSLV***X***GF***i***TYLTNLYFKIREDRRKAARGE
	i-4	MRYIRSDKISTGIAYGTSAGSAGYWFLQWLDQVSPSQWAAIGVLGSL***X***LGF***i***TYLTNLYFKIREDRRKAARGE

This table shows the primary sequence of active S^{21}68 and inactive S^{21}IRS pinholin. The deuterated Leu (d_{10}Leu) position is denoted by '**i**' while the position of the cysteine substitution is shown as ***X***. The underlined sections of the primary sequence correspond to the two predicted transmembrane domains.

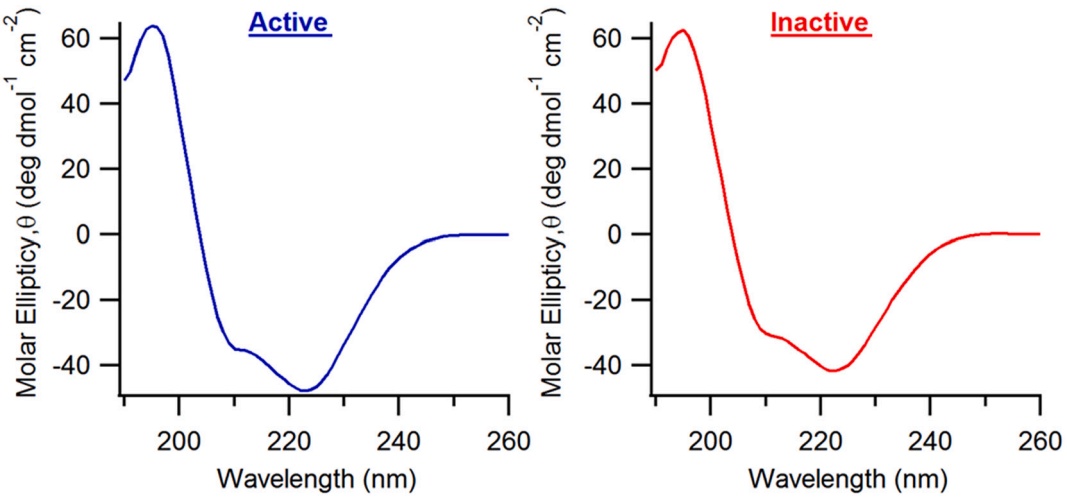

Fig. 1. Representative CD spectra of the active (blue) and inactive (red) forms of the pinholin S^{21} confirming α-helical secondary structure with spin label and deuterated amino acid sidechains. (For interpretation of the references to colour in this figure legend, the reader is referred to the web version of this article.)

step wise away from the d_{10}-Leu sidechain. In a helix, when the spin label is at a position 2 amino acids away from the d_{10}-Leu, the spin label and the d_{10}-Leu appear on opposite sides on the helix and therefore outside of the 8 Å ESEEM detection limit. As the spin label is moved to positions 3 or 4 amino acids away from the d_{10}-Leu, the helical structure puts both labels on the same side of the helix allowing for deuterium modulation to be observed [8]. Alternatively, the exact opposite pattern would be detected when probing a β-sheet. The linear nature of β-sheets would place the spin label within the detection limit at position 1 or 2 amino acids away from the d_{10}-Leu allowing for deuterium modulation. Unlike the α-helix, there would be no deuterium modulation detected at positions 3 and 4 amino acids away from the d_{10}-Leu as the linear β-stand would place the spin label more than 8 Å away from the d_{10}-Leu. To this point the application of the ESEEM technique has been limited to model peptides or small protein segments of known structure [6,8]. This study will be the first application of the outlined ESEEM approach to a full-length membrane protein with multiple predicted transmembrane domains (TMDs).

The final step of the double-stranded DNA bacteriophage infection cycle is host lysis [15]. The mechanism for this lysis pathway involves three proteins, a small hole-forming inner membrane protein known as the holin, a muralytic enzyme known as the endolysin, and the spanin complex responsible for outer membrane disruption. The function of the holin protein is to permeabilize the inner cytoplasmic membrane, depolarizing the membrane, and allowing the release of the endolysin to begin the degradation of the peptidoglycan [16]. This is accomplished by a harmless accumulation of the holin in the host cell membrane until the protein "triggers" at an allele-specific time. Triggering is the term used to denote when the holin reaches a critical concentration in the membrane and attains the functionality to permeabilize the membrane. Due to the variation in mechanisms and sizes of lesions formed between different classes of holins the lesions have been termed "holes" to show distinction from channels and other such membrane permeabilization pathways [3,17,18].

This study will focus on a cytosolic membrane protein known as pinholin S^{21}, encoded by the S^{21} holin gene of the lambdoid bacteriophage Φ21 [16]. Pinholin S^{21} is one of the most well-studied prototype holin system which make nanoscale holes to dissipate the proton motive force (PMF) in the inner cytosolic membrane of the infected bacteria to release and activate the membrane-tethered signal anchor release (SAR) endolysin to degrade the peptidoglycan layer [16,19–22]. Pinholin S^{21} has two holin proteins; active pinholin and inactive antipinholin. Both pinholin S^{21} proteins have two TMDs [21]. TMD1 of the active form of pinholin rapidly externalized from the inner cytoplasmic membrane to the periplasm and facilitated the oligomerization of TMD2 to form a nano-scale hole. However, TMD1 of the inactive form of pinholin cannot or slowly externalize from the inner cytoplasmic membrane due to the extra positive charge and bulky side-chains in the N-terminal. Hence,

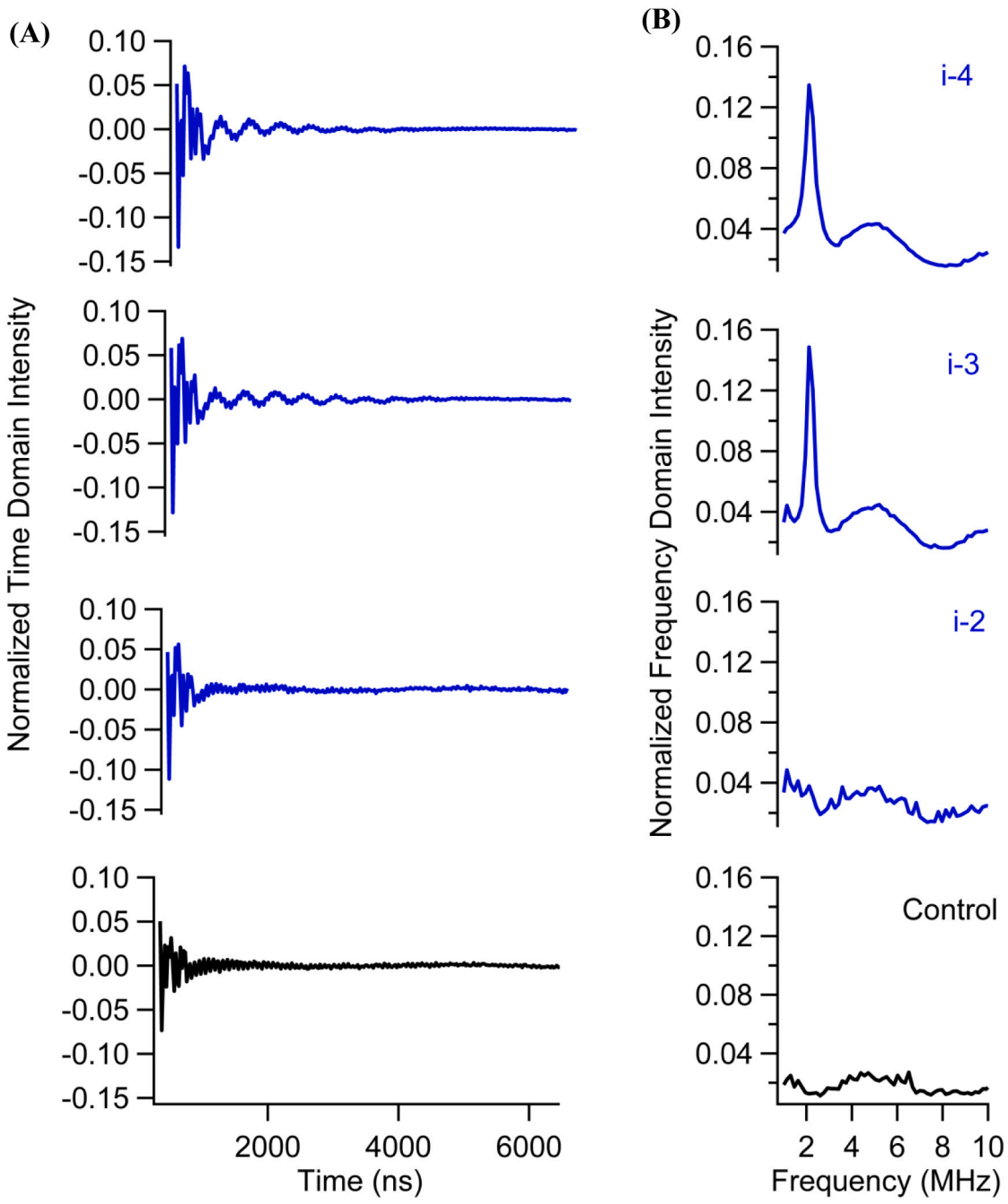

Fig. 2. Three pulse ESEEM experimental data for the active form of pinholin S^{21} with ^{2}H labeled Leu (d_{10}-Leu) side chain at position 25 in TMD1 incorporated in DMPC liposomes at 1:500 protein to lipid ratio. ^{2}H modulation can be observed in the time domain (A) at positions i-4 and i-3 which translates to the peaks seen in the normalized frequency domain intensity (B). The frequency domain data is normalized to make the same maximum scale for each set of data.

prevent the oligomerization of TMD2 to form the nano-scale holes. The S^{21}68 is the active form of the pinholin S^{21}, while the S^{21}IRS will represent the inactive antipinholin form [23]. S^{21}IRS has five extra amino acids (RYIRS) between the first methionine (M) and the second aspartic acid (D) of active pinholin. Until this point the predicted helical secondary structure has only been hypothesized using molecular dynamic simulations and through comparison to other classes of holin proteins [17]. The work presented here will be the experimental evidence to confirm the local secondary structure of full length pinholin S^{21} in its active and inactive conformations.

2. Experimental methods

All pinholin S^{21} proteins were synthesized using solid phase peptide synthesis conducted on a CEM Liberty Blue Peptide Synthesizer with Discovery Bio Microwave System [24,25]. Thirteen different variants of the active and inactive forms were created to complete the study including a control construct without deuterated amino acid. Table 1 outlines all twelve different deuterated and spin labeled pinholin positions.

These pinholin constructs were generated to position a deuterated leucine (d_{10}-Leu) amino acid at a specific position designated as **i**. A cysteine residue, denoted in Table 1 as ***X***, is then substituted in at specific position −2, −3, or −4 residues away from the deuterated leucine,

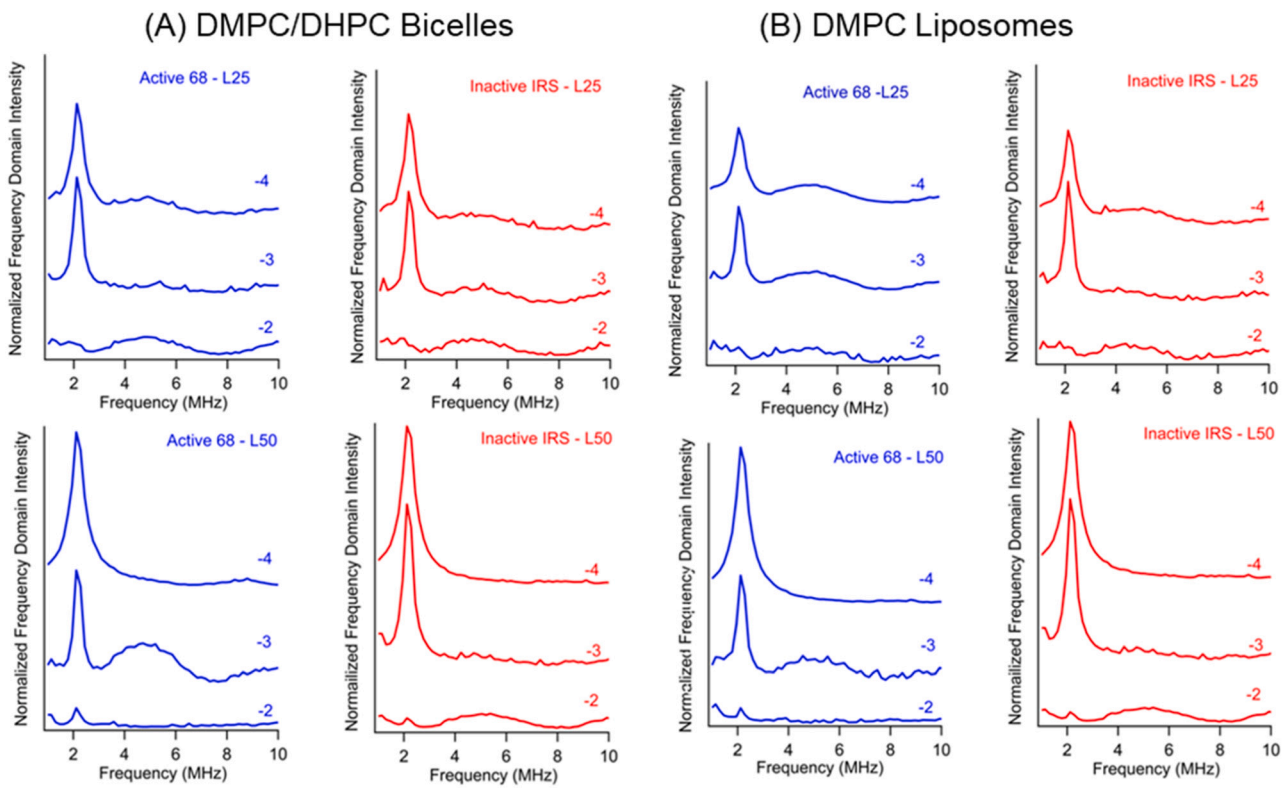

Fig. 3. (A) Normalized ^{2}H frequency domain intensity for active pinholin S^{21}68 (blue) and inactive antipinholin S^{21}IRS (red) for TMD1 (top) and TMD2 (bottom) in DMPC/DHPC bicelles (B) Normalized ^{2}H frequency domain intensity for active pinholin S^{21}68 (blue) and inactive antipinholin S^{21}IRS (red) for TMD1 (top) and TMD2 (bottom) in DMPC liposomes. The frequency domain intensity was normalized to get maximum scale to make a relative comparison of the peak intensity among i-2, i-3, and i-4 samples of each site. (For interpretation of the references to colour in this figure legend, the reader is referred to the web version of this article.)

i. This cysteine residue allows for disulfide bond formation to the nitroxide spin label MTSL to ensure the pinholin S^{21} is EPR active. A control sample was synthesized by creating an i-4 pinholin with a natural (undeuterated) leucine side chain at position Leu25.

After successful solid phase synthesis, the pinholin S^{21} was cleaved from the solid phase resin using a trifluoroacetic acid (TFA) cleavage solution and crude peptide was obtained following previously published optimized cleavage procedure [25–27]. The crude pinholin was purified using reverse-phase high performance liquid chromatography (RP-HPLC) with a C4 prep column run at a gradient of 5 to 95% solvent B (90% acetonitrile/10% water/0.1% TFA) [25–28]. The collected pure peptide fractions were lyophilized, and the resulting pure peptide was spin labeled using MTSL [26]. Spin labeled peptide was repurified using reverse-phase HPLC to remove the excess spin label. This purification was run using a C4 semi-prep column with the same gradient and solvent system as previously mentioned [25–27]. Matrix assisted laser desorption ionization – time of flight (MALDI-TOF) was used to confirm the target molecular weight of the pinholin S^{21} plus successful MTSL coupling. All the remaining pure, spin labeled pinholin S^{21} fractions were lyophilized into a powder to use for lipid incorporation and the resulting experiments [23].

The pure spin labeled pinholin S^{21} was incorporated into two different lipid mimetic systems at a 500:1 lipid to protein ratio. The final protein concentration was 200 μM. 1,2-Dimyristoyl-sn-Glycero-3-Phosphocholine (DMPC)/1,2-Diheptanoyl-sn-Glycero-3-Phosphocholine (DHPC) bicelles were created by mixing the two lipids, dissolved in chloroform, with a Q value of 3.6 and then adding the corresponding amount of pinholin S^{21} dissolved in 2,2,2-Trifluoroethanol (TFE). The solvents were evaporated off using inert N_2 gas and the remaining lipid/protein film was rehydrated using 20 mM HEPES (4-(2-hydroxyethyl)-1-piperazineethanesulfonic acid) buffer adjusted to a neutral pH of ~7.0. The lipid/protein solution was flash frozen in liquid nitrogen and then vortexed and sonicated until the buffer solution went clear. The second lipid mimetic used were multilamellar vesicles (MLVs) created by mixing the peptide dissolved in 2,2,2-Trifluoroethanol (TFE) with DMPC in chloroform at a 500:1 lipid to protein ratio. Then the solvents were evaporated off using inert N_2(g) and the same process as bicelle formation was followed with a minimum of three freeze thaw cycles.

The global secondary structure was determined using circular dichroism (CD) spectroscopy performed on an Aviv Circular Dichroism Spectrometer Model 435 in a quartz cuvette with a 1.0 mm path length. CD data was collected from 260 to 190 nm with 1 nm bandwidth at 25 °C.

X-band CW-EPR (~9 GHz) spectra were used to calculate spin labeling efficiency with all samples showing greater than 85% labeling efficiency. Three-pulse (π/2-τ-π/2-T-π/2) ESEEM measurements were conducted on a Bruker ELEXSYS E580 with an ER4118X MS3 resonator using a 200 ns tau value for ^{1}H modulation suppression. The ESEEM data for each sample was collected at a microwave frequency of ~9.269 GHz and a magnetic field of ~3300 G at a temperature of 80 K with 4-step phase cycling. The spectra were collected with a starting T value of 386 ns with an increase in 12 ns increments for a total of 512 points [6,7]. All ESEEM data were collected on a 45 μL sample incorporated into either 500:1 DMPC MLVs or 500:1 DMPC/DHPC bicelles. A two-component exponential decay was used to fit the time domain data. The maximum value for the exponential fit as well as the collected time domain data were both scaled to one, according to the literature [29]. The normalized decay curve was subtracted from the experimental data to give a scaled ESEEM spectrum [30–32]. A Fourier Transformation (FT) was then applied to the scaled ESEEM spectra to yield the corresponding frequency domain [33]. The detected deuterium peak appears at ~2.3 MHz corresponding to the Larmor frequency of ^{2}H.

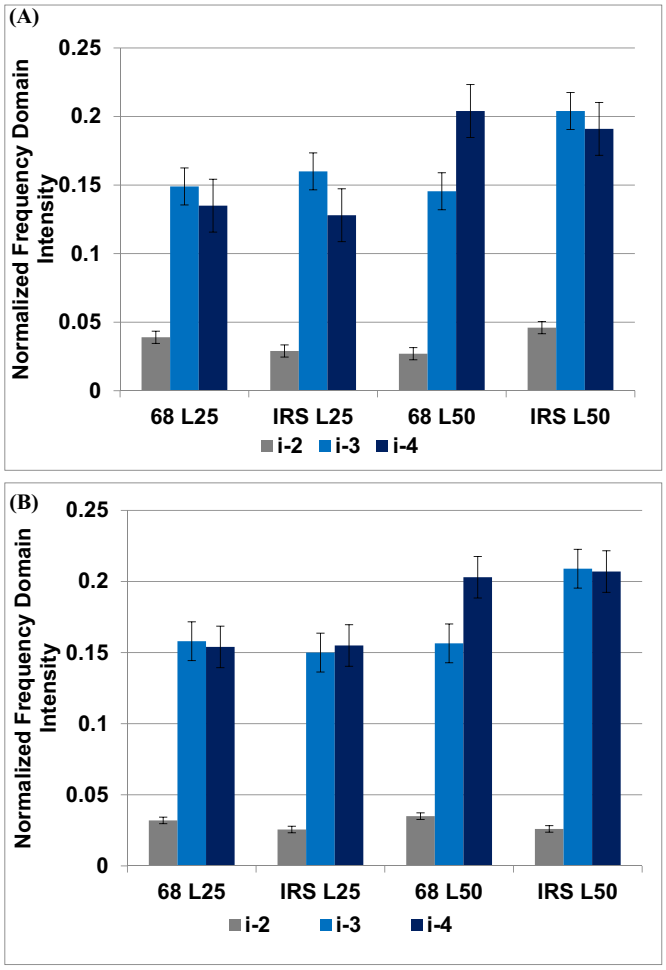

Fig. 4. Comparison of normalized frequency domain intensity for both TMDs of the active and inactive forms of pinholin S^{21} in (A) DMPC/DHPC bicelles at a 1:500 ratio Figs. 1:, 2:, 3: and 4: and (B) DMPC liposomes at a 1:500 ratio.

3. Results and discussion

In the pathway of bacteriophage cell lysis, the pinholin S^{21} protein is responsible for the permeabilization of the inner cell membrane and the overall timing of the lysis mechanism [19,22]. In this study, CD spectroscopy as well as an established 3-pulse ESEEM approach were used to investigate both global and local secondary structure of pinholin S^{21} within the membrane. Fig. 1 shows representative CD spectra of the active (blue) and inactive (red) forms of deuterated and spin labeled versions of pinholin S^{21}. In both cases, we saw a large positive peak below 200 nm and double minima at 208 and 222 nm corresponding to a global α-helical secondary structure.

Following the confirmation of the global secondary structure for the active and inactive pinholin S^{21} the ESEEM approach outlined above was used to probe the local secondary structure. Positions were chosen within both transmembrane regions predicted by the literature to be helical in nature for both the active and inactive forms of the pinholin [20]. Position L25 is located in the first predicted TMD while L50 is located in the second predicted TMD. The ESEEM detected modulation can be seen in the i-3 and i-4 positions of the time domain of Fig. 2A with a frequency of 2.2 MHz corresponding to the Larmor frequency of deuterium. This modulation results in a ^2H peak that can be observed in the i-3 and i-4 positions of the spin label in Fig. 2B.

The presence of the deuterium peak at positions i-3 and i-4 with the absence of the peak at i-2 is indicative of α-helical secondary structure for Leu25 [7,34,35]. This pattern comes from the 3.6 amino acid turn periodicity of the α-helical secondary structure. This places the spin label, at i-3 and i-4, and the deuterated leucine side chain on the same face of the helix allowing dipolar coupling, while the i-2 position falls on the opposite face of the helix outside of the 8 Å detection limit [36]. Fig. 3 shows the normalized frequency intensity for all data collected in DMPC/DHPC 1:500 bicelles (A) left and DMPC 1:500 liposomes (B) right.

The helical pattern can be observed when looking at deuterated position L25 located in TMD1 (top row) for both the S^{21}68 active (blue) and the S^{21}IRS inactive (red). This helical secondary structure is also present in the functional domain TMD2 of the pinholin S^{21}. This is seen at the bottom row of Fig. 3 with deuterated position L50 showing deuterium dipolar coupling peaks for the i-3 and i-4 positions but not for i-2.

A comparison of the normalized FT frequency domain intensity was conducted and plotted in Fig. 4. Due to unique turn periodicities for different helices, such as 3.1 amino acids for a 3_{10} helix or 4.1–4.4 amino acids for a π helix, comparing the normalized frequency domain intensity will allow for differentiation between these helices [6,37,38].

A minor peak was observed in some of the samples might be due to the interaction of spin label with a small amount of ^2H sidechain or unfolded protein [36]. There is some variation present in the intensity between each position because of two distinct reasons. The first comes from the differences in the local environment between TMD1 and TMD2 and how that environment influences the mobility and packing of the spin label and d_{10}-Leu side chain. The second is due to the presence of the multiple torsion angles in the longer side chains, like leucine, and the MTSL-labeled cysteine of which there are 5 torsion angles χ1–5 [17,19,20,24,39,40]. The comparison of intensities between the i-3 and i-4 peaks for bicelles incorporated pinholin S^{21} samples yields close frequency peak intensities for them. Similarly, the comparison of intensities between the i-3 and i-4 peaks for the liposome incorporated pinholin S^{21} samples also yield close frequency peak intensities. These results suggest that TMD1 (Leu 25) and TMD2 (Leu 50), for both the active and inactive forms of the pinholin S^{21}, are folded in an α-helical secondary structure. The result of this study along with our previous studies will serve as a data library for utilizing this ESEEM approach for studying more complicated protein systems.

4. Conclusions

Determining the secondary structure of membrane proteins is pivotal in understanding protein functions and dynamics. Techniques such as CD spectroscopy can give global secondary structure information but lack the ability to specify local secondary structural information. As opposed to techniques like NMR which require higher sample concentrations, longer data acquisition time, and are restricted by protein size, this ESEEM approach requires only μM scale of a sample, shorter data acquisition (~2 h to a few hrs) and has no limit on protein size. The ESEEM method is easy to apply for synthetic peptides. However, this method has been also applied to larger membrane proteins and soluble proteins. Another powerful EPR spectroscopic technique, DEER can measure long-range (20–80 Å) distances and predict secondary structure, while ESEEM can provide more direct evidence of local secondary structure and differentiate among the secondary structures. The application of ESEEM outlined in this paper demonstrated the ability to probe local secondary structure, not only for model peptides as previously published but of full-length functional systems. The α-helical local secondary structure of both predicted pinholin S^{21} TMDs were confirmed with the presence of deuterium modulation observed at the i-3 and i-4 positions [12]. The confirmation of the helical structure in TMD1 and TMD2 for both the active and inactive forms of the pinholin S^{21} demonstrates the applicability of this technique to both peripheral and internal membrane proteins. In addition, the comparison of frequency domain intensities between the active and inactive conformations indicates there is little to no change in helical structure after TMD1

externalizes from the membrane. Future application of this work will include application at helical boundaries to observe the loss of helical folding pattern to identify the end point of the helix. This ESEEM approach will be utilized to probe tertiary interactions of functional systems known to form dimers or oligomeric states and the use of deuterated buffers to probe membrane protein topology.

Declaration of competing interest

Gary Lorigan reports financial support was provided by NIGMS. Gary Lorigan reports financial support was provided by NSF.

Data availability

Data will be made available on request.

Acknowledgment

This work was generously supported by the NSF CHE-1807131 grant. The pulsed EPR spectrometer used to conduct the experiments was purchased through the NSF and the Ohio Board of Reagents grants (MRI-0722403). Gary A. Lorigan would also like to acknowledge support from the John W. Steube Professorship. Indra D. Sahu would also like to acknowledge support from the NSF MCB-2040917 award.

Appendix A. Supplementary data

Supplemental Information includes figures for relative positions of the deuterated Leu (d_{10}Leu) and MTSL in active and inactive conformations of pinholin, CW-EPR spectra, and three pulse ESEEM experimental data. Supplementary data to this article can be found online at https://doi.org/10.1016/j.bbamem.2021.183836.

References

[1] R. Lappano, M. Maggiolini, G protein-coupled receptors: novel targets for drug discovery in cancer, Nat. Rev. Drug Discov. 10 (1) (2011) 47–60.
[2] C.S. Tautermann, GPCR structures in drug design, emerging opportunities with new structures, Bioorg. Med. Chem. Lett. 24 (17) (2014) 4073–4079.
[3] R. Young, Phage lysis: three steps, three choices, one outcome, J. Microbiol. 52 (3) (2014) 243–258.
[4] N. Bordag, S. Keller, Alpha-helical transmembrane peptides: a "divide and conquer" approach to membrane proteins, Chem. Phys. Lipids 163 (1) (2010) 1–26.
[5] C.D. Huang, S. Mohanty, Challenging the limit: NMR assignment of a 31 kDa helical membrane protein, J. Am. Chem. Soc. 132 (11) (2010) 3662–3663.
[6] L. Bottorf, S. Rafferty, I.D. Sahu, R.M. McCarrick, G.A. Lorigan, Utilizing electron spin echo envelope modulation to distinguish between the local secondary structures of an alpha-helix and an amphipathic 3(10)-helical peptide, J. Phys. Chem. B 121 (14) (2017) 2961–2967.
[7] L.S. Liu, G. Lorigan, Probing the secondary structure of membrane proteins with the pulsed EPR ESEEM technique, Biophys. J. 106 (2) (2014) 192A.
[8] L.S. Liu, I.D. Sahu, L. Bottorf, R.M. McCarrick, G.A. Lorigan, Investigating the secondary structure of membrane peptides utilizing multiple H-2-labeled hydrophobic amino acids via electron spin echo envelope modulation (ESEEM) spectroscopy, J. Phys. Chem. B 122 (16) (2018) 4388–4396.
[9] G.A. Lorigan, Probing the structure of membrane proteins with ESEEM and DEER pulsed EPR techniques, Biophys. J. 102 (3) (2012) 423A.
[10] N. Kurochkina, Helix-helix interactions and their impact on protein motifs and assemblies, J. Theor. Biol. 264 (2) (2010) 585–592.
[11] M. Gross, Proteins that convert from alpha helix to beta sheet: implications for folding and disease, Curr. Protein Pept. Sci. 1 (4) (2000) 339–347.
[12] T. Kubota, J.J. Lacroix, F. Bezanilla, A.M. Correa, Probing alpha-3(10) transitions in a voltage-sensing S4 helix, Biophys. J. 107 (5) (2014) 1117–1128.
[13] R. Carmieli, N. Papo, H. Zimmermann, A. Potapov, Y. Shai, D. Goldfarb, Utilizing ESEEM spectroscopy to locate the position of specific regions of membrane-active peptides within model membranes, Biophys. J. 90 (2) (2006) 492–505.
[14] L. Sun, J. Hernandez-Guzman, K. Warncke, OPTESIM, a versatile toolbox for numerical simulation of electron spin echo envelope modulation (ESEEM) that features hybrid optimization and statistical assessment of parameters, J. Magn. Reson. 200 (1) (2009) 21–28.
[15] R. Young, I. Wang, Phage lysis, in: The Bacteriophages, 2nd ed., Oxford Univ Press, Oxford, 2006.
[16] T. Park, D.K. Struck, C.A. Dankenbring, R. Young, The pinholin of lambdoid phage 21: control of lysis by membrane depolarization, J. Bacteriol. 189 (24) (2007) 9135–9139.
[17] T. Pang, C.G. Savva, K.G. Fleming, D.K. Struck, R. Young, Structure of the lethal phage pinholin, PNAS 106 (45) (2009) 18966–18971.
[18] R. Young, Phage lysis: do we have the hole story yet? Curr. Opin. Microbiol. 16 (6) (2013) 1–8.
[19] T. Pang, T. Park, R. Young, Mapping the pinhole formation pathway of S21, Mol. Microbiol. 78 (3) (2010) 710–719.
[20] T. Pang, T. Park, R. Young, Mutational analysis of the S21 pinholin, Mol. Microbiol. 76 (1) (2010) 68–77.
[21] T. Pang, C.G. Savva, K.G. Fleming, D.K. Struck, R. Young, Structure of the lethal phage pinhole, Proc. Natl. Acad. Sci. U. S. A. 106 (45) (2009) 18966–18971.
[22] T. Pang, T.C. Fleming, K. Pogliano, R. Young, Visualization of pinholin lesions in vivo, Proc. Natl. Acad. Sci. U. S. A. 110 (22) (2013) E2054–E2063.
[23] D.L. Drew, T. Ahammad, R.A. Serafin, B.J. Butcher, K.R. Clowes, Z. Drake, I. D. Sahu, R.M. McCarrick, G.A. Lorigan, Solid phase synthesis and spectroscopic characterization of the active and inactive forms of bacteriophage S-21 pinholin protein, Anal. Biochem. 567 (2019) 14–20.
[24] S. Chandrudu, P. Simerska, I. Toth, Chemical methods for peptide and protein production, Molecules 18 (4) (2013) 4373–4388.
[25] T. Ahammad, D.L. Drew, I.D. Sahu, R.A. Serafin, K.R. Clowes, G.A. Lorigan, Continuous wave electron paramagnetic resonance spectroscopy reveals the structural topology and dynamic properties of active pinholin S(21)68 in a lipid bilayer, J. Phys. Chem. B 123 (38) (2019) 8048–8056.
[26] D.L. Drew Jr., T. Ahammad, R.A. Serafin, B.J. Butcher, K.R. Clowes, Z. Drake, I. D. Sahu, R.M. McCarrick, G.A. Lorigan, Solid phase synthesis and spectroscopic characterization of the active and inactive forms of bacteriophage S21 pinholin protein, Anal. Biochem. 567 (2018) 14–20.
[27] T. Ahammad, D.L. Drew, R.H. Khan, I.D. Sahu, E. Faul, T. Li, G.A. Lorigan, Structural dynamics and topology of the inactive form of S21 holin in a lipid bilayer using continuous-wave electron paramagnetic resonance spectroscopy, J. Phys. Chem. B 124 (26) (2020) 5370–5379.
[28] D.J. Mayo, J.J. Inbaraj, N. Subbaraman, S.M. Grosser, C.A. Chan, G.A. Lorigan, Comparing the structural topology of integral and peripheral membrane proteins utilizing electron paramagnetic resonance spectroscopy, J. Am. Chem. Soc. 130 (30) (2008) 9656–9657.
[29] M. Heming, M. Narayana, L. Kevan, Analysis of nuclear-quadrupole interaction effects in electron spin-echo modulation spectra by 2nd-order perturbation-methods, J. Chem. Phys. 83 (4) (1985) 1478–1484.
[30] L. Urban, H.J. Steinhoff, Hydrogen bonding to the nitroxide of protein bound spin labels, Mol. Phys. 111 (18–19) (2013) 2873–2881.
[31] A.D. Milov, R.I. Samoilova, A.A. Shubin, E.Y. Gorbunova, L.G. Mustaeva, T. V. Ovchinnikova, J. Raap, Y.D. Tsvetkov, Self-aggregation and orientation of the ion channel-forming zervamicin IIA in the membranes of ePC vesicles studied by CW EPR and ESEEM spectroscopy, Appl. Magn. Reson. 38 (1) (2010) 75–84.
[32] R. Bartucci, R. Guzzi, L. Sportelli, D. Marsh, Intramembrane water associated with TOAC spin-labeled alamethicin: electron spin-echo envelope modulation by D2O, Biophys. J. 96 (3) (2009) 997–1007.
[33] S. Stoll, R.D. Britt, General and efficient simulation of pulse EPR spectra, Phys. Chem. Chem. Phys. 11 (31) (2009) 6614–6625.
[34] A.D. Zhou, S. Abu-Baker, I.D. Sahu, L.S. Liu, R.M. McCarrick, C. Dabney-Smith, G. A. Lorigan, Determining alpha-helical and beta-sheet secondary structures via pulsed electron spin resonance spectroscopy, Biochemistry 51 (38) (2012) 7417–7419.
[35] R.F. Zhang, I.D. Sahu, K.R. Gibson, N.B. Muhammad, A.P. Bali, R.G. Comer, L. S. Liu, A.F. Craig, R.M. McCarrick, C. Dabney-Smith, C.R. Sanders, G.A. Lorigan, Development of electron spin echo envelope modulation spectroscopy to probe the secondary structure of recombinant membrane proteins in a lipid bilayer, Protein Sci. 24 (11) (2015) 1707–1713.
[36] J.A. Cieslak, P.J. Focia, A. Gross, Electron spin-echo envelope modulation (ESEEM) reveals water and phosphate interactions with the KcsA potassium channel, Biochemistry 49 (7) (2010) 1486–1494.
[37] P. Kumar, M. Bansal, Dissecting pi-helices: sequence, structure and function, FEBS J. 282 (22) (2015) 4415–4432.
[38] B.W. Low, R.B. Baybutt, The PI-helix - a hydrogen bonded configuration of the polypeptide chain, J. Am. Chem. Soc. 74 (22) (1952) 5806–5807.
[39] L. Columbus, T. Kalai, J. Jeko, K. Hideg, W.L. Hubbell, Molecular motion of spin labeled side chains in alpha-helices: analysis by variation of side chain structure, Biochemistry 40 (13) (2001) 3828–3846.
[40] L. Columbus, W.L. Hubbell, A new spin on protein dynamics, Trends Biochem. Sci. 27 (6) (2002) 288–295.